THEORETICAL AND EXPERIMENTAL INVESTIGATIONS ON A SPECIAL ROTARY PIEZOELECTRIC MOTOR WITH TUBULAR GEOMETRY

George C. ZĂRNESCU[1]

Această lucrare descrie o abordare teoretică şi experimentală asupra unui motor piezoelectric cu geometrie tubulară. Teoria este dezvoltată pornind de la ecuaţiile de bază ale piezoelectricităţii pentru efectul direct şi invers scris sub formă tensorială şi ecuaţiile diferenţiale ale deplasărilor şi tensiunilor mecanice radiale şi circumferenţiale. Aceste ecuaţii sunt combinate într-o modelare matematică care împreună cu simulările 3D ale mişcării mecanice descriu întreaga interacţiune electromecanică. Secţiunile următoare se concentrează asupra metodelor de acţionare, a caracteristicilor şi performanţelor motorului. Influenţa frecvenţei şi a forţelor axiale este comparată atât theoretic cât şi experimental.

This paper describes an experimental and theoretical approach on a rotary piezoelectric motor with tubular geometry. Theory is developed starting from the basic piezoelectric equations of direct and inverse piezoelectric effect written in tensorial form and the differential equations of inner radial and circumferential mechanical stresses and deformations. These equations are combined in one modelling type and 3D simulations of mechanical movement to give a description of the entire electromechanical interaction. Next sections concentrate on the driving methods, electromechanical characteristics and performances. The influence of frequency and axial forces is compared both theoretically and experimentally.

Keywords: piezoelectric, tubular, waves, resonance

1. Introduction

Many types of piezoelectric micromotors have been constructed by now starting from the idea of ultrasonic electromechanical conversion of electrical energy into useful mechanical thrust.

Among them, a micromotor with cylindrical stator shape and panhead or spherical rotor is studied here. The micromotor is described also in national patent no. 122516 / 2007 granted to the author.

The working principle of this piezoelectric motor can be explained in single phase supply by Rayleigh surface waves motion. The elliptical waves are produced at stator-rotor contact surface when the tubular piezoceramic element is

[1] Eng., INCDIE ICPE CA, Dept. of Electrical Engineering, University POLITEHNICA of Bucharest, Romania, e-mail: zgcnet@yahoo.com

excited by a sinusoidal voltage at resonant frecquency. The rotor is forced to move by friction forces in the opposite travelling wave direction. This type of ultrasonic micromotor has the advantage of a simple manufacturing technology, compactness, large axial force support at low angular speed and a good precision and control. Two major disadvantages are the reliability for long operation due to friction and the need for an ultrasonic frequency power supply with at least 25 V peak voltage.

Section 2 describes the micromotor construction and the principle of operation. In section 3 we propose a mathematical modeling algorithm accurate enough to predict the real time motor performances. Section 4 concentrates on the experimental work, the basic micromotor functional characteristics, mechanical and electrical parameters determination, different vibration modes and frequency variation intervals settings. Section 5 makes a comparison between theoretical and experimental results and part 6 concludes the paper.

2. Tubular micromotor construction and operating principle

In Fig. 1 is shown the structure of the tubular piezoelectric motor. The operation of rotary piezoelectric micromotor is based on surface progressive waves generation in piezoceramic materials.

Rotary piezoelectric micromotor is composed from a tubular piezoceramic stator (1) having a diameter between 11-28 mm and a length between 10-20 mm, a compression system (2), a conical or spherical rotor (4), shaft (5), a screw nut (6), a bearing system (9), stator support (3), electrical wiring (7), inner and outer cylindrical conductive surface (8) and case (10), see Fig. 1.

Two versions of this motor with similar geometry where constructed, a smaller one with an outside diameter of 15 mm and 10 mm height (MPR15) and the other having an outside diameter of 33 mm, an inner diameter of 25 mm and height of 20 mm (MPR33). Piezoceramic cylinder can be supplied either from a single phase, either by a biphasic voltage source, generating a mechanical progressive wave at ultrasonic frequencies that is rotating the conical or spherical rotor. Movement is transmitted through direct mechanical contact between the upper part of piezoelectric cylinder and rotor conical surface. The compression system with a spring, nut and bolt is adjusting the contact pressure between the pan head rotor and the piezoceramic cylinder, mounted on the stator support using also the rotor shaft and the ball bearing system at the bottom. Electrical connections are soldered to four external cylindrical electrodes for a biphasic supply and the inner cylindrical electrode is considered null. Electrodes are made from a conductive silver lake applied on piezoceramic tube.

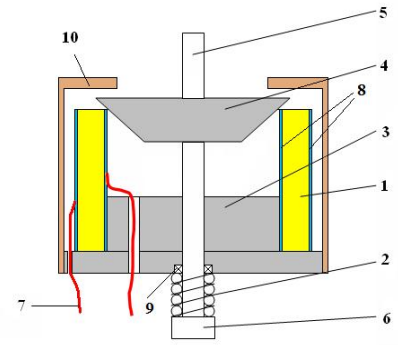

Fig. 1. Section through rotor and stator of piezoelectric converter

In a single phase supply mode, micromotor operation can be explained with the help of Rayleigh surface waves. The basic principle is to produce elliptical waves at stator-rotor interface. When tubular piezoceramic element is excited by a sinusoidal voltage signal it will produce a longitudinal vibration along radial direction. Since the pan head rotor has an angle of 45 degrees of the slope (or is spherical) the impact between tubular converter and rotor will be inclined, causing a secondary axial vibration. Radial vibration and axial (transversal) one will compose resulting in an elliptical motion at the contact surface of between stator and rotor.

In bi-phased regime, these two waves are created directly by 90 degrees electrical phase shifting. The two stationary waves are composed resulting a elliptical movement trajectory of the surface points. This wave will interact with rotor generating a rotation movement [3].

3. Theoretical modelling and simulations

For this tubular piezoelectric converter we have developed a mathematical model that is accurate enough to predict its real behavior and performances. Equations are used in mathematical modeling or for a preliminary actuator design. Each piezoelectric constant is in fact a tensor and is describing the effect on each polar or Cartesian coordinate.

First of all we must take in consideration the geometry and all mechanical stresses for our piezoceramic element. Mechanical stresses can be either external, either internal. External forces balance is derived from classical mechanics. A more complicated way is to determine the internal mechanical stress inside piezoelectric material. This is where differential equations of material science interfere with both classical mechanics and piezoelectricity.

Because electric displacement field doesn't have any component along the axial direction, we can consider that the mechanical stress on that axis is zero.

Also other projections that are not from the established polar coordinate system are nullified. The only remaining mechanical stresses and most important are radial and circumferential ones.

General mechanical stress equations can be simplified and reformed because of tubular geometry (relation 1). Shear stress and circumferential angle θ dependence are excluded from further calculation.

$$\frac{\partial \sigma_{rr}}{\partial r} + \frac{\sigma_{rr} - \sigma_{\theta\theta}}{r} = 0 \tag{1}$$

This first equation is rewritten to take in account equilibrium and compatibility conditions. The result is a system of partial derivatives from that the solution is extracted. Differential equations solving is skipped due complexity and space limitation. In the end the solution looks like:

$$\begin{cases} \sigma_{rr} = \dfrac{a^2 p_i}{b^2 - a^2}\left(1 - \dfrac{b^2}{r^2}\right) \\ \sigma_{\theta\theta} = \dfrac{a^2 p_i}{b^2 - a^2}\left(1 + \dfrac{b^2}{r^2}\right) \end{cases}, \tag{2}$$

Where *a* is inner radius, b outer radius, p_i the pressure given from rotor to stator inner surface, and $\sigma_{rr}, \sigma_{\theta\theta}$ are radial and circumferential stresses. This inner pressure and frictional forces are dependent mainly on rotor weight and other axial loads. Outer surface pressure is considered zero, no external force is acting on that surface.

So, we can see that radial and circumferential stresses $\sigma_{rr}, \sigma_{\theta\theta}$ are changing with inverse square radius. This dependence takes into account the piezoceramic element geometry and will be further used to replace stresses in piezoelectricity relations.

If equation of compatibility is ignored then equilibrium equations system will give multiple solutions. So, compatibility equation and pressure boundary conditions are generating unique solutions (see system 2).

The connection between mechanical stress and deformation for an usual material is just Hook's law, but for a piezoelectric material Hook's law must be extended and integrated to form general equations of piezoelectricity.

In our particular case of a piezoceramic cylinder, radial and circumferential mechanical stress dependence function of deformation and electric field can be written in 3D polar coordinates like:

$$\begin{aligned}\sigma_{\theta\theta} &= c_{11}L_{\theta\theta} + c_{12}L_{rr} - n_{31}E_r \\ \sigma_{rr} &= c_{12}L_{\theta\theta} + c_{33}L_{rr} - n_{33}E_r\end{aligned} \tag{3}$$

L-specific deformation relative to geometric dimension $[\frac{\Delta x}{x}]$; s-compliance $[\frac{m^2}{N}]$; d-piezoelectric charge accumultation coefficient [m/V or C/N], σ-mechanical stress; ε-total electrical permitivity; E-applied electrical field [V/m];

Stiffness c is the reciprocal of compliance s, $c = s^{-1}$, n is another piezoelectric constant and is directly connected to compliance s and piezoelectric charge or polarization coefficient d by $d = n \cdot s$ or $n = d \cdot c$ relations. Even if we don't know the stiffness and the electric field constant, we can express them by the other coefficients d and s (charge coefficient and compliance). Comsol calculation was made using the same system (3).

For PZT5 material relative constants are:

$d_{31} = -171, \quad d_{33} = 374, \quad d_{15} = 584, \quad \varepsilon_{11} = 1730, \quad \varepsilon_{33} = 1700$

$s_{11} = 16.4, \quad s_{33} = 18.8, \quad s_{13} = -5.74, \quad s_{12} = -7.22$

Absolute values are:

$s_{ij}^* = s_{ij} \cdot 10^{-12} \frac{m^2}{N}, d_{ij}^* = d_{ij} \cdot 10^{-12} \frac{C}{N}, \varepsilon_{ij}^* = \varepsilon_{ij} \cdot 8.85 \cdot 10^{-12} \frac{F}{m}.$

In analogue mode, knowing that there is no dependence of θ variable for radial and circumferential deformations and shear deformation is eliminated due to symmetry, we can ignore any partial derivative of circumferential angle θ.

$$\begin{cases} L_{\theta\theta} = \dfrac{u_r}{r} \\ L_{rr} = \dfrac{\partial u_r}{\partial r} \\ \gamma_{r\theta} = 0 \end{cases} \tag{4}$$

$L_{\theta\theta}$ – relative circumferential deformation; L_{rr} – relative radial deformation; u_r – radial deformation, $\gamma_{r\theta}$ – shearing deformation.

General equation of mechanical equilibrium and piezoelectric equations must be satisfied in any case. So, replacing radial and angular mechanical stresses from equation 2, with general piezoelectric expressions from system 3 we obtain a complete differential equation of relative deformations that can be resolved. But

relative radial and circumferential deformations are directly changing with the real radial displacement, like we see in system 4. If we further replace relative radial and angular displacements from system 4 to the final differential equation we will have a single variable to resolve. After another derivation of r radius and expression rearrangements we will have the radial displacement equation.

A simplified solution of radial displacement is showed below (see also Fig. 2, [1]):

$$u_r = Ar + \frac{B}{r} + s_{11}\frac{d_{33}s_{31} - d_{31}s_{33}}{s_{31}s_{33}}E_r \tag{5}$$

Initially we have solved mechanical stress expressions for our tubular geometry, now a simple way to calculate A and B constants from radial displacement equation 5 is to impose boundary conditions $\sigma_{rr}(a) = -p_i$, $\sigma_{rr}(b) = 0$, $\sigma_{\theta\theta}(a) = \frac{b^2 + a^2}{b^2 - a^2}p_i$, $\sigma_{\theta\theta}(b) = \frac{2a^2}{b^2 - a^2}p_i$ and to replace mechanical stresses from system 2, more exactly into secondary equation [1]. So, after this arithmetic artifice the full expression of radial displacement is finally revealed.

$$A = \frac{(s_{33} + s_{12})\cdot a^2 p_i}{b^2 - a^2} + d_{33}E_r \qquad B = \frac{(s_{33} - s_{12})\cdot a^2 b^2 p_i}{b^2 - a^2} \tag{6}$$

Above we have showed a static solution model that is highly accurate in comparison with some other types of electromechanical modelling. If we need an immediate answer on piezoelectric motor behaviour maybe is more proper to work with electromechanical schemes and impedances at resonance frequency. This other electromechanical approach can give faster results but is not accurate enough, unless is improved by further additions. A static model can be useful but is more interesting to estimate the dinamic behaviour of rotary piezoelectric motor. For this we need to focus on ultrasonic wave propagation.

We start from a simplified version of general wave propagation equation written in polar coordinates (equation 7). Using variable separation method for radial, circular displacement and time, a solution of wave propagation is described in expression 8.

$$\frac{\partial^2 u}{\partial t^2} = v_0^2\left(\frac{\partial^2 u}{\partial r^2} + \frac{1}{r}\frac{\partial u}{\partial r}\right) \tag{7}$$

$$u(r,t) = K_r \cdot u_r \cdot \cos(\omega t - k\theta) \tag{8}$$

$K_r = \left(\frac{r-a}{b-a}\right)^N$ is a factor (modal factor) that depends on vibration mode and piezoceramic element geometry, $2^{1/2}$ in our case of first vibration mode and cylinder average radius, ω – angular frequency.

$$v = \frac{\partial u}{\partial t} = -K_r \cdot u_r \cdot f \cdot \sin(\omega t - k\theta) \tag{9}$$

Linear speed v of the transverse traveling wave was written as a displacement variation with time. A maximum value of angular speed corresponds to a maximum linear speed and to a maximum variation of the radial deformation.

Angular speed obtained by calculation from relation 10 is greater than the one determined by experimental means at mechanical resonance frequency of 159 kHz, approximate five times greater than electrical frequency of 32000 Hz. 3D simulation model will be confirmed also by simulations (same displacements).

$$n = \frac{60}{2\pi}\frac{v_m}{a} = \frac{60}{2\pi}\frac{K_r u_t f}{a} \tag{10}$$

In reality radial vibrations u_r and axial vibrations u_z are combined resulting an overall displacement u_t, $u_t = \sqrt{u_r^2 + u_z^2}$. The maximum rotational speed n is estimated to 16 rpm (from the wave movement, we need a correction parameter for the rotor movement).

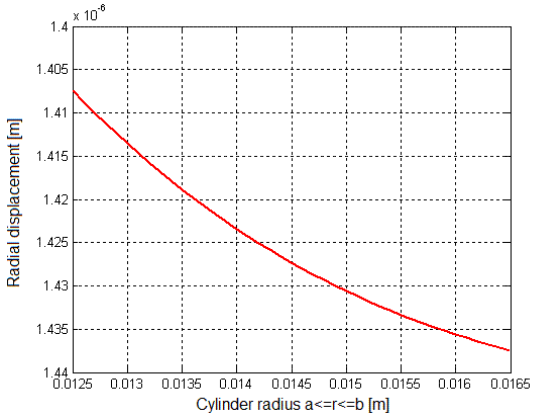

Fig. 2. Radial displacement variation for MPR 33 function of cylinder radius

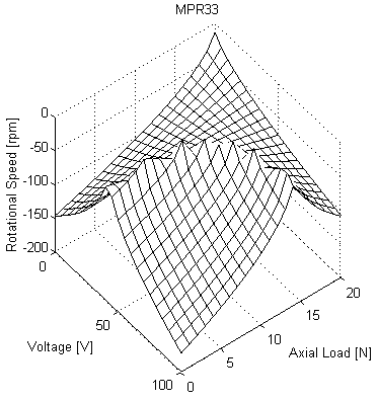

Fig. 3. Angular speed estimation function of voltage and axial force

For a voltage that varies between $0 \div 100\,V$ and an axial force being in $0 \div 20\,N$ range, applying radial displacement solution from equation 5 and calculating expression 10 we can approximately estimate the maximum angular speed. Speed can be calculated for any voltage and axial force.

A maximum deformation of cylinder means also a maximum amplitude for ultrasonic wave and angular speed. Cylinder deformation was also simulated using COMSOL program. At different moments of time that can be established geometrically where maximum and minimum radial and axial displacements can appear. This is a dynamic simulation closely related to real situation. We know that at $t = 0$ we have $\sin(k\theta) = 1 \Rightarrow k\theta = \pi/2$. Every separation limit of two neighbor electrodes with $\pi/2$ diphase geometrically and electrically gets maximum displacements (Fig. 4).

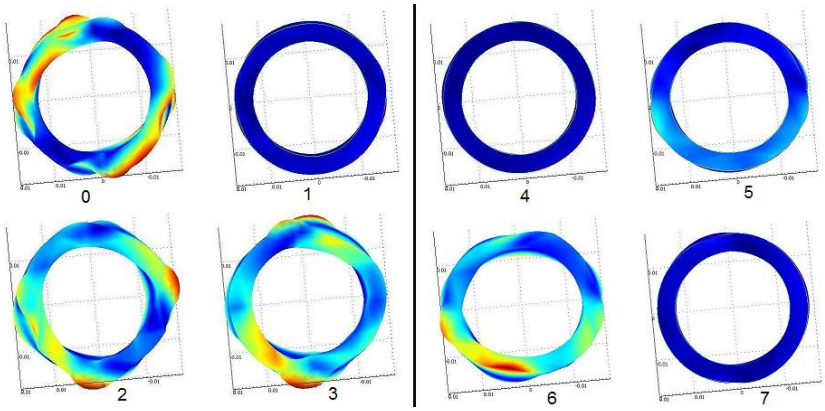

Fig. 4. MPR33 cylinder deformation at different oscillating times 0,1/8, 2/8....8/8*T, coresponding to period T

Fig. 4 simulates cylinder deformation using (-Sin)(-Cos)(Sin)(Cos) diphase voltage supply, creating a progressive wave inside piezoelectric material [4]. All inner surface is connected to the ground. We can observe that we have eight main steps in order to complete a full osicllating period. Each step corresponds to an angle in radians $0(2\pi),\frac{\pi}{4},\frac{\pi}{2},\frac{3\pi}{4},\pi,\frac{5\pi}{4},\frac{3\pi}{2},\frac{7\pi}{4}$. At zero time coordinate or full period $\mathrm{T}(2\pi)$ we have a maximum amplitude of 50 V and at 1 and 5 positions, respectively 45° and 225°, we obtain quite uniform stresses for the entire tubular geometry. The maximum displacement is $0.6\ \mu m$ and each of four sectors is electrically supplied with $0.707 \cdot U$ voltage.

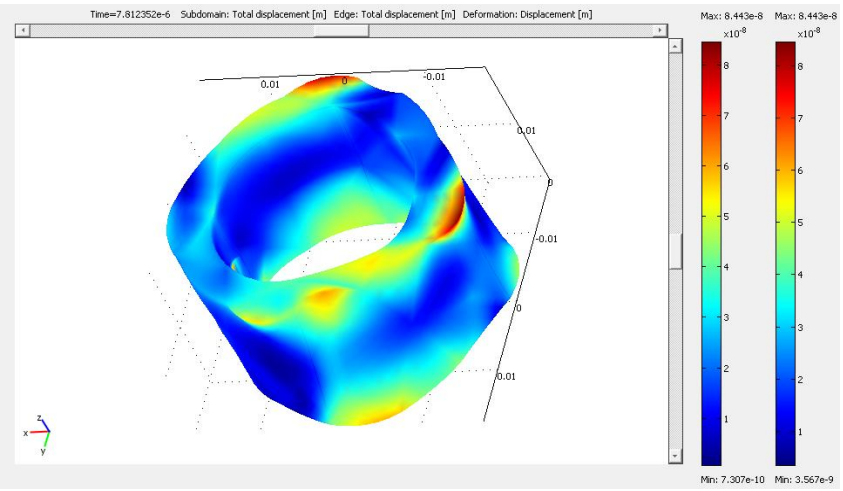

Fig. 5. 3D simulation of total cylinder deformation at 2T/8 period of time, the point where cosinus is minimum and sinus is maximum

At π angle it is peak value of $1.18\ \mu m$ for deformation, meaning that the cosinusoidal signal is reaching the voltage limit of 50 V. For $\pi/2$ angle or $2T/8$ position, altough we obtain only $0.0844\ \mu m$, we clearly see that zones supplied with sinusoidal signal are the most stressed and the ones of cosinusoidal signal don't have any vibrations (see Fig. 5). The red spots are maximum deformation zones, green and yellow zones are under average or little above average and blue or dark blue zones are the minimum deformations zones. Main deformation zones are localized on cylinder edges or at separation limit between sectors.

All simulations where realized using basic equations and constant matrix values that are presented in chapter 3.

4. Experimental micromotor characteristics and functional parameters determination

Experimental tests were focused on resonance frequency identification, different vibration modes and variation intervals, torque and friction forces analysis, determination of main working motor characteristics, like speed control function of frequency at constant torque and voltage or axial force and contact pressure influence on piezoelectric motor speed and overall performances.

Motor speed is controlled from a variable frequency source with a maximum voltage amplitude of 50 V.

In Fig. 6 a) and 6 b) are presented two characteristics, one for MPR33 motor and the other for MPR15, of angular speed variation function of frequency. Characteristics are determined for different axial loads, 6 N and 4 N, in case of MPR33 tests or 0.23 N and 1.73 N (spherical rotor weights), for the case of MPR15.

An important observation in both cases is the rapid variation of angular speed for a relative narrow frequency range. For MPR33 the frequency variation interval is between 32 and 33.5 kHz and for MPR15 between 22 and 23 kHz. At the end of both intervals motor speed is very low or practically zero. In the middle of angular speed variation curve will reach a maximum value, 9 rpm for MPR33 and 8 rpm for MPR15.

Experimental curves have a maximum at 32700 Hz resonance frequency for MPR33 and 22200 Hz for MPR15 model. Axial force modification gives a resonance point displacement of about 100 Hz down with the increase of axial load from 6 N to 4 N. This can be explained as a changing in mass for the entire stator-rotor electromechanical system and also a microcontact variation.

Vibration transmission from piezoelectric converter to rotor is realized by micromechanical contact. So, we must find the best available microcontact for an efficient electromechanical conversion. This can be done when we find an optimal pressure and of course an optimal axial force. In this way can be explained the apparent anomaly of axial force and angular speed dependence.

Electrical resonance frequency is different from mechanical resonance frequency. So, when we talk about resonance and frequency control it is all about the electrical frequency responsible for mechanical resonance. By analogy, once the axial force is increasing and is over the optimal value, rotor speed will tend to decrease. By axial force variation we also have obtained an angular speed curve similar to a Bode diagram. Lower axial forces as also higher axial forces compared to the optimal axial force value give us a poor functional efficiency, this can be directly observed from speed variation in Fig. 7 a).

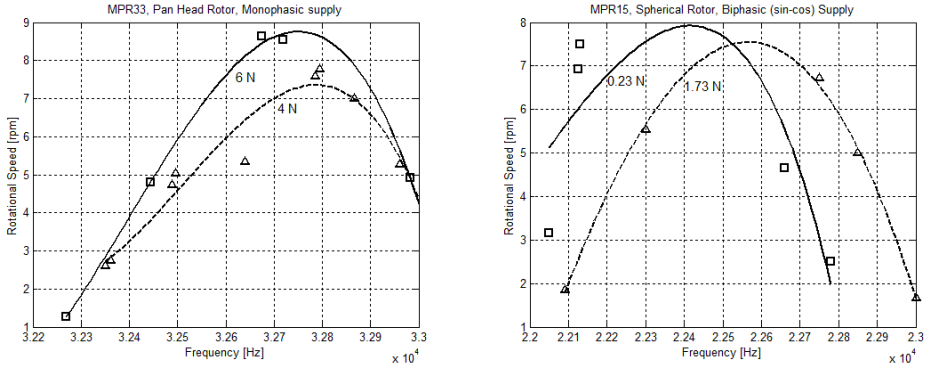

a) **b)**

Fig. 6. a) Speed function of frequency characteristics for MPR33 motor with pan head rotor, at 6 N and 4 N axial loads; b) Speed function of frequency characteristics for MPR15 motor with spherical rotors having 0.23 N and 1.73 N loads

When we totally exceed these limits the rotor will stop rotating. For an axial force under 1 N the rotor doesn't have a good contact pressure and friction force, so the electromechanical energy transfer is lost. In the same way, for an axial force that exceeds the upper limit of 18 N, dynamic friction is so high that all electromechanical energy is consumed by it, effective force generated by the piezoceramic tube is much under dynamic friction force and the rotor will stop. In the transmission of movement by mechanical contact we will always need the friction force as a binding element between two surfaces.

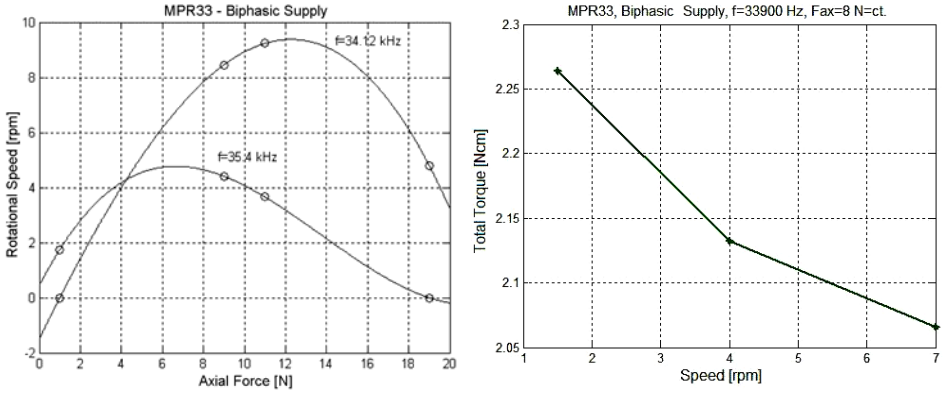

a) **b)**

Fig. 7. a) Rotational speed variation for different axial forces at two distinct resonance points of MPR33; b) Total MPR33 torque function of rotational speed, mechanical characteristic around resonance frequency

In our case the dynamic friction force directly depends on the axial force variation from the first law of motion $F_f = \mu_k \sqrt{2} \cdot F_{ax}$, so in this way we can explain the motor behaviour at different axial loads.

From previous diagrams we can conclude that speed regulation and control can be realized either by frequency variation, either by changing the contact pressure and axial force [5].

Mechanical characteristic is quite flexible permitting a speed variation between 0 and 10 rpm. Friction torque is between 0.2..0.3 cNm.

5. Comparison between theoretical and experimental results

We saw from previous sections that piezoelectric displacement plays an important role in estimating motor behaviour [6, 7]. The influence is very simple because deformation is linearly increasing with voltage and angular speed depends on vibration amplitude and frequency. In order to measure micrometric and nanometric displacements we need special devices like a linear laser interferometer or a feed finger. A laser interferometer uses two optical paths and laser beams to be compared and to extract the nanometric displacement. It is sufficient for the moving probe to change the path of one laser beam when a retroreflector is fixed on it. Axial displacement was measured for the entire frequency interval. It is interesting to observe that a maximum displacement appears only at resonance frequency. This experimental evidence shows us that even if an ultrasonic motor is supplied by a significant voltage the piezoelectric effect is minimum outside resonance frequency.

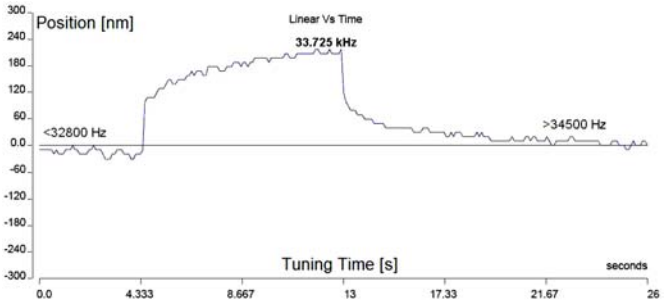

Fig. 8. MPR33 axial displacement at resonant 33.7 kHz frequency

Three conditions must be respected for this type of ultrasonic motor to work: voltage must be high enough to ensure an optimum displacement, frequency must be around resonance point and contact pressure or force must be carefully chosen for optimum performances.

Below is a comparison table of measured and calculated displacement values near resonance frequency. Peak to peak voltage is 45 V and axial force is 3 N, both are kept constant to ensure the same conditions.

Table 1

Measured and calculated displacements

MPR33 PZT-5 Material	Measured axial displacement [nm]	Calculated axial displacement [nm]	Measured radial displacement [μm]	Calculated radial displacement [μm]
Uvv=ct.=45 V F=ct.=3 N	220	150	2	1.44

We see that are no major differences between theoretical and experimental results for radial and axial displacements.

Modifying axial force and keeping the voltage constant at 50 V for tubular piezoceramic element will give us a speed variation like in Fig. 9. For a frequency of 31250 Hz that is little under resonance we still observe a maximum angular speed of 4.5 rpm. If we increase the axial force from 2 N up to 8 N we sense that the rotor is significantly slowing down until it stops. At this frequency the motor has poor performances and supports only lower axial forces. Theoretical and experimental results are quite similar. The first curve from Fig. 7 a) shows us an apparent anomaly, that the speed is increasing together with force or torque.

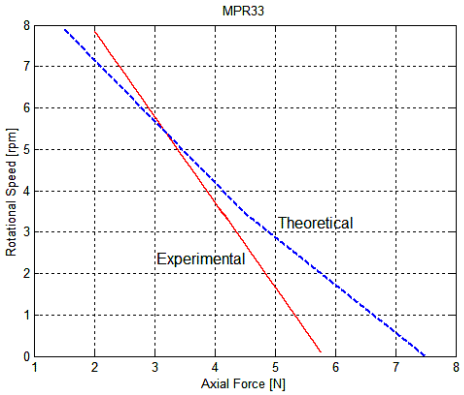

Fig. 9. Theoretical and experimental angular speed characteristics function of applied axial force.

If both torque and speed are increasing means also that we've got more mechanical output power. A possible explanation is that efficiency is increasing and losses are diminished. It is obvious that when we reach to an optimum axial load the motor efficiency is increasing because of a larger developed microdisplacement and a mechanical contact improvement.

6. Conclusions

Using a laser interferometer we were able to determine the resonance modes with 10 nm precision. Submicronic measured axial displacement of 220 nm could be compared with the theoretical axial displacement value of 150 nm. For a 50 V peak to peak voltage a radial displacement of maximum $2\,\mu m$ was obtained. We can conclude that the MPR model is mainly based on radial and axial vibrations of piezoelectric tube to generate movement.

All the experimental work was done to improve the overall motor performances and obviously to establish the optimum working point, that corresponds to a 12 N axial force and to a maximum rotational speed of 9 rpm.

We also saw that motor performances are drastically changing with frequency. Even if we shift frequency with only some hundred Hertz from resonant point, the angular speed is decreasing until the rotor stops. For an electrical drive system voltage, axial force and frequency can be used for an automatic control of angular speed. Axial force or contact pressure can be modified by a secondary linear actuator (piezoelectric or electromagnetic). In most cases voltage combined with frequency control is preferred.

Almost all theoretical results are confirmed by experiments so we can conclude that our proposed mathematical model is sufficiently accurate to predict motor behavior around resonance.

REFERENCES

[1] *Chen Ying, Shi Zhi-fei,* "Analysis of a functionally graded piezothermoelastic hollow cylinder", Journal of Zhejiang University Science, 2005, **6A**, pag. 956-961

[2] *T. Cimprich, F. Kaegi, W. Driesen*, „Ultrasonic monolithic piezoelectric multi DOF actuators for mobile microrobots", 10th International Conference on New Actuators (**Actuator 2006**) Proceedings, p.114-117

[3] *P. Juang, G. Da-Wei*, „Analysis, measurement and control of a new disc-type ultrasonic motor system", Mechatronics, **Vol 16**, Issue 1, February 2006, p. 1-12

[4] *O. Holub, T. Cimprich, A. Ferreira,* „Dynamical modelling and position control of ultrasonic monolithic piezoelectric actuator for mobile microrobots", **IEEE International Ultrasonic Symposium**, Vancouver, Canada, October 3-6 2006

[5] *M. Ignat, G. Zărnescu,* "Comparative Study on The Equivalent Circuit of The Electric Motor and Traveling Wave Piezoelectric Ultrasonic Motor", **ICEM 2006**, Chania, Crete Island, Greece, 2-5 Sept. 2006

[6] *M. Cazacu, M. Ignat, C. Racles, G. Zărnescu*, "Polydimethylsiloxane/silica composites incorporating pyrite powders for actuation elements", Polymer International, **Vol. 58**, Nr. 7, Pag. 745-751, Iul. 2009

[7] *M. Cazacu, M. Ignat, A. Vlad, M. Alexandru, G. Zărnescu*, „Heat-cured silicone rubber incorporating pyrite powders for actuation elements", Optoelectronics and Advanced Materials-Rapid Communications, **Vol. 4**, Nr. 3 , Pag. 349-351, Mar. 2010